The Eurasia Proceedings of Science, Technology, Engineering & Mathematics (EPSTEM)
ISSN: 2602-3199

The Eurasia Proceedings of Science, Technology, Engineering and Mathematics (EPSTEM), 2025

Volume 38, Pages 264-275

IConTES 2025: International Conference on Technology, Engineering and Science

Effect of the Strain Rate and Temperature on the Shape Memory Behavior of PMMA

Cherief Mohammed Nadhir Djamel Eddine
Djilali Liabes University of Sidi Bel Abbes

Ghermaoui Ilias Mohammed Amine
Djilali Liabes University of Sidi Bel Abbes

Abstract: In the field of smart materials, significant scientific progress has been made over the past decade on shape memory polymers (SMPs), which appear to offer numerous advantages. Their ability to change shape under the influence of an external stimulus, such as thermal, presents a certain interest for biomedical applications and the deployment of structures. In this section, we will develop a thermoviscoelastic-viscoplastic model to predict the shape memory behavior of poly (methyl methacrylate) (PMMA) and understand its thermomechanical behavior over a wide range of strain rate and temperatures.

Keywords: SMP, Strain rate, Temperature, Polymers, PMMA

Introduction

The industrial development of polymers, commonly known as plastics, has experienced remarkable growth since the last century. Today, the annual global production of polymers by volume exceeds that of metals. This evolution explains the growing interest in studying the behavior of these materials within the research community. Polymers are used in a wide variety of sectors. Packaging, whether for food or household products, represents the largest share of plastic consumption. Next come the fields of construction, automotive, household appliances, textiles, and electricity. Moreover, more specialized sectors such as medicine and aeronautics have also shown a strong interest in these materials.

PMMA, thanks to its transparency and high rigidity, is one of the most widely used technical polymers. It is found in most of the sectors mentioned above, particularly in applications where impact resistance is crucial, such as in the manufacture of windshields or the transparent covers of high-speed machine tool housings (UGV). The behavior of PMMA strongly depends on its processing history, the nature and rate of deformation, as well as temperature, with a significant thermomechanical coupling. Based on these observations, we chose to focus our work on the experimental and theoretical study of the rheology of PMMA. This study aims to analyze its behavior through simple uniaxial compression tests and then compare the results with the predictions of a model we have developed.

The shape memory effect refers to the ability of a material to retain a stable deformation within a certain temperature range and then recover its original shape when subjected to an external stimulus. Several types of stimuli can activate this shape memory in polymers, including water, heat, ultraviolet radiation, or electricity. In applications exploiting the shape memory of polymers, the development of constitutive models is highly sought after to provide essential tools for design. Constitutive modeling is crucial due to the complexity of the behavior associated with the shape memory effect. Although literature abounds with experimental studies on this phenomenon, modeling remains a major challenge for better understanding and controlling these materials.

Method

To illustrate our approach a polycarbonate ($T_g \gg 413K$), was selected for an experimental test program under uniaxial compression. Compression specimens of 8.00 mm length and 6.3 mm diameter were machined from PMMA cylinders. The length to-diameter ratio of the specimens allows getting the stress-strain response at large strains by avoiding both buckling and non-homogeneous deformation. Lubricant was used between the platens and the specimen surfaces (smooth and parallel) to avoid both barreling and shearing phenomena during the compression. The experiments were carried out on an electromechanical model-5567 Instron universal testing machine equipped with an oven.

- Loading-unloading tests until zero stress: The specimens were loaded at a constant strain rate until a prescribed strain and then unloaded at the same absolute strain rate until zero stress. The tests were conducted at different strain rates, above and below T_g.
- Creep tests at zero stress of pre-deformed specimens: The specimens, previously deformed below T_g, were cooled to the room temperature T_0 by natural cooling and then submitted to creep experiments at zero stress for two different temperatures above T_g.

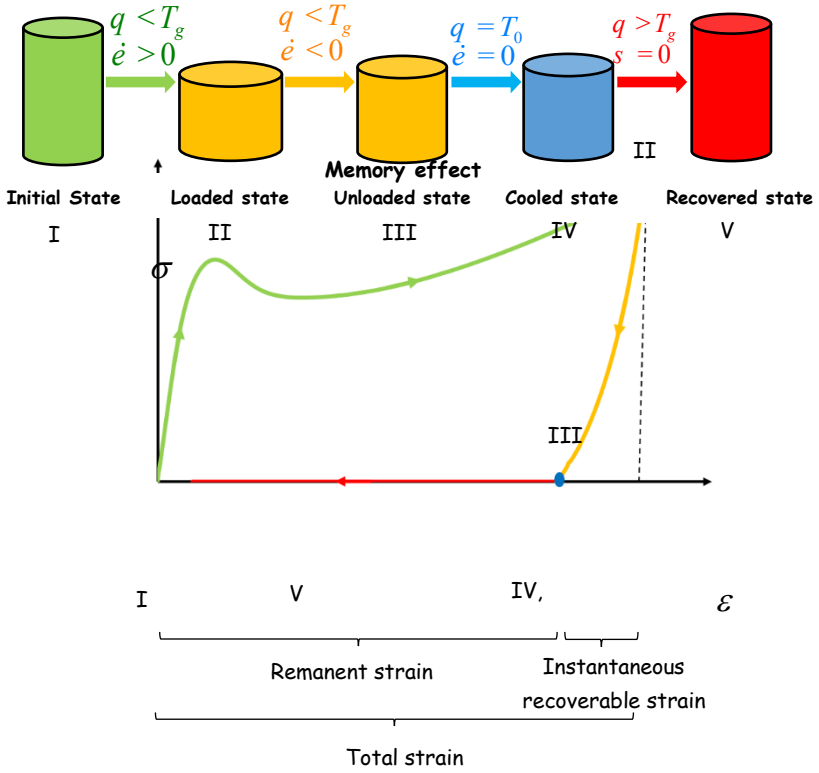

Figure 1. Elastoviscoplastic-viscohyperelastic response of an amorphous polymer below T_g under a loading-unloading compression experiment and recovery of the remanent strain under a creep test at zero stress above T_g.

Theory

The monotonic response of an amorphous polymer can be related to two underlying physical mechanisms acting in parallel: The first one is an intermolecular resistance to chain-segment rotation (resistance I) and the second one is a molecular network resistance due to molecular orientation (resistance N). The resistance I is the source of the initial stiffness and the yield events, whereas the resistance N is the source of the dramatic strain hardening at large strains. The constitutive equations of the resistance I are formulated using the elastoviscoplastic theory and those of the resistance N are formulated using the viscohyperelastic theory.

Kinematics

The total deformation gradient $\mathbf{F}$ can be multiplicatively decomposed as:

$$\mathbf{F} = \mathbf{F}_q \mathbf{F}_M \tag{1}$$

in which $\mathbf{F}_\theta$ is the thermal part related to stress-free thermal expansion and $\mathbf{F}_M$ is the mechanical part related to the isothermal stress-producing contribution.

The Taylor assumption imposes that the intermolecular and network deformation gradients, $\mathbf{F}_I$ and $\mathbf{F}_N$, are both equal to the mechanical deformation gradient $\mathbf{F}_M$:

$$\mathbf{F}_M = \mathbf{F}_I = \mathbf{F}_N \tag{2}$$

The two deformation gradients, $\mathbf{F}_I$ and $\mathbf{F}_N$, can be multiplicatively decomposed into elastic and inelastic parts:

$$\mathbf{F}_I = \mathbf{F}_I^{\mathrm{e}} \mathbf{F}_I^{\mathrm{vp}} \tag{3}$$

$$\mathbf{F}_N = \mathbf{F}_N^{\mathrm{h}} \mathbf{F}_N^{\mathrm{v}} \tag{4}$$

where the superscripts e, vp, h and v denote the elastic, viscoplastic, hyperelastic and viscous flow parts, respectively. The different parts can be further decomposed into rotation and stretch components:

$$\mathbf{F}_I^{\mathrm{e}} = \mathbf{R}_I^{\mathrm{e}} \mathbf{U}_I^{\mathrm{e}} = \mathbf{V}_I^{\mathrm{e}} \mathbf{R}_I^{\mathrm{e}} \text{ and } \mathbf{F}_I^{\mathrm{vp}} = \mathbf{R}_I^{\mathrm{vp}} \mathbf{U}_I^{\mathrm{vp}} = \mathbf{V}_I^{\mathrm{vp}} \mathbf{R}_I^{\mathrm{vp}} \tag{5}$$

$$\mathbf{F}_N^{\mathrm{h}} = \mathbf{R}_N^{\mathrm{h}} \mathbf{U}_N^{\mathrm{h}} = \mathbf{V}_N^{\mathrm{h}} \mathbf{R}_N^{\mathrm{h}} \text{ and } \mathbf{F}_N^{\mathrm{v}} = \mathbf{R}_N^{\mathrm{v}} \mathbf{U}_N^{\mathrm{v}} = \mathbf{V}_N^{\mathrm{v}} \mathbf{R}_N^{\mathrm{v}} \tag{6}$$

The intermolecular and network velocity gradients, $\mathbf{L}_I$ and $\mathbf{L}_N$, are described by:

$$\mathbf{L}_I = \underbrace{\dot{\mathbf{F}}_I^{\mathrm{e}} \mathbf{F}_I^{\mathrm{e}^{-1}}}_{\mathbf{L}_I^{\mathrm{e}}} + \underbrace{\mathbf{F}_I^{\mathrm{e}} \dot{\mathbf{F}}_I^{\mathrm{vp}} \mathbf{F}_I^{\mathrm{vp}^{-1}} \mathbf{F}_I^{\mathrm{e}^{-1}}}_{\mathbf{L}_I^{\mathrm{vp}}} \tag{7}$$

$$\mathbf{L}_N = \underbrace{\dot{\mathbf{F}}_N^{\mathrm{h}} \mathbf{F}_N^{\mathrm{h}^{-1}}}_{\mathbf{L}_N^{\mathrm{h}}} + \underbrace{\mathbf{F}_N^{\mathrm{h}} \dot{\mathbf{F}}_N^{\mathrm{v}} \mathbf{F}_N^{\mathrm{v}^{-1}} \mathbf{F}_N^{\mathrm{h}^{-1}}}_{\mathbf{L}_N^{\mathrm{v}}} \tag{8}$$

The inelastic velocity gradients, $\mathbf{L}_I^{\mathrm{vp}}$ and $\mathbf{L}_N^{\mathrm{v}}$, may be both decomposed as the sum of symmetric and skew-symmetric parts:

$$\mathbf{L}_I^{\mathrm{vp}} = \mathbf{F}_I^{\mathrm{e}} \mathbf{F}_I^{\mathrm{vp}} \mathbf{F}_I^{\mathrm{vp}^{-1}} \mathbf{F}_I^{\mathrm{e}^{-1}} = \mathbf{D}_I^{\mathrm{vp}} + \mathbf{W}_I^{\mathrm{vp}} \tag{9}$$

$$\mathbf{L}_N^{\mathrm{v}} = \mathbf{F}_N^{\mathrm{h}} \mathbf{F}_N^{\mathrm{v}} \mathbf{F}_N^{\mathrm{v}^{-1}} \mathbf{F}_N^{\mathrm{h}^{-1}} = \mathbf{D}_N^{\mathrm{v}} + \mathbf{W}_N^{\mathrm{v}} \tag{10}$$

in which $\mathbf{D}$ is the symmetric part and $\mathbf{W}$ is the skew-symmetric part. The intermolecular and network inelastic flows are assumed to be irrotational, i.e. $\mathbf{W}_I^{\mathrm{vp}} = \mathbf{0}$ and $\mathbf{W}_N^{\mathrm{v}} = \mathbf{0}$. Moreover, $\mathbf{D}_I^{\mathrm{vp}}$ and $\mathbf{D}_N^{\mathrm{v}}$ are constitutively given in the next subsection.

Constitutive Model Formulation

The Taylor assumption imposes that the total Cauchy stress $\boldsymbol{\sigma}$ is the sum of both contributions:

$$\boldsymbol{\sigma} = \boldsymbol{\sigma}_I + \boldsymbol{\sigma}_N \tag{11}$$

where $\boldsymbol{\sigma}_I$ is the intermolecular Cauchy stress and $\boldsymbol{\sigma}_N$ is the network Cauchy stress.

Elastoviscoplastic Response: Stiffness and Plastic Yielding

The yield behavior of amorphous polymers is a thermally-activated process. The intermolecular Cauchy stress $\boldsymbol{\sigma}_I$ is expressed by the following constitutive relationship:

$$\boldsymbol{\sigma}_I = \frac{\mathbf{C}_I^{\mathrm{e}}}{J_I} \ln\left(\mathbf{V}_I^{\mathrm{e}}\right) \tag{12}$$

in which $J_I = \det\left(\mathbf{F}_I^{\mathrm{e}}\right)$ is the intermolecular volume change, $\ln\left(\mathbf{V}_I^{\mathrm{e}}\right)$ is the Hencky elastic strain and $\mathbf{C}_I^{\mathrm{e}}$ is the elastic stiffness tensor. In the isotropic case, the elastic stiffness tensor $\mathbf{C}_I^{\mathrm{e}}$ may be given in terms of the Young's modulus E and the Poisson's ratio ν as follows:

$$\left(\mathbf{C}_I^{e}\right)_{ijkl} = \frac{E\left(q,\dot{e}\right)}{2\left(1+n\left(q,\dot{e}\right)\right)}\left(d_{ik}d_{jl} + d_{il}d_{jk}\right) + \frac{2n\left(q,\dot{e}\right)}{1-2n\left(q,\dot{e}\right)} d_{ij}d_{kl} \tag{13}$$

in which the term d denotes the Kronecker-delta symbol. The stiffness of polymers is clearly temperature-dependent as shown in Fig. 2. The thermo-dependence is due to … Moreover, it depends on the strain-rate. The evolution of the Young's modulus is given by the following expression (Richeton et al., 2005b):

$$E\left(q,\dot{e}\right) = E_{T_b}\left(q,\dot{e}\right) + E_{T_g}\left(q,\dot{e}\right) + E_{T_m}\left(q,\dot{e}\right) \tag{14}$$

in which $E_{T_b}\left(q,\dot{e}\right)$, $E_{T_g}\left(q,\dot{e}\right)$ and $E_{T_m}\left(q,\dot{e}\right)$ correspond to three parts around the main transitions (β relaxation, glass transition and melting) which are characterized by their transition temperatures, T_b, T_g and T_m:

$$E_{T_b}\left(q,\dot{e}\right) = \left(E_1\left(\dot{e}\right) - E_2\left(\dot{e}\right)\right)\exp\left(-\left(\frac{q}{T_b\left(\dot{e}\right)}\right)^{m_1}\right) \tag{15}$$

$$E_{T_g}\left(q,\dot{e}\right) = \left(E_2\left(\dot{e}\right) - E_3\left(\dot{e}\right)\right)\exp\left(-\left(\frac{q}{T_g\left(\dot{e}\right)}\right)^{m_2}\right) \tag{16}$$

$$E_{T_m}\left(q,\dot{e}\right)=E_3\left(\dot{e}\right)\exp\left(-\left(\frac{q}{T_m\left(\dot{e}\right)}\right)^{m_3}\right) \tag{17}$$

where m_1, m_2 and m_3 are material constants and, $E_1\left(\dot{e}\right)$, $E_2\left(\dot{e}\right)$ and $E_3\left(\dot{e}\right)$ are the instantaneous moduli at the beginning of each transition region:

$$E_1\left(\dot{e}\right)=E_{1ref}\left(1+s_1\log\left(\frac{\dot{e}}{\dot{e}_{ref}}\right)\right) \tag{18}$$

$$E_2\left(\dot{e}\right)=E_{2ref}\left(1+s_2\log\left(\frac{\dot{e}}{\dot{e}_{ref}}\right)\right) \tag{19}$$

$$E_3\left(\dot{e}\right)=E_{3ref}\left(1+s_3\log\left(\frac{\dot{e}}{\dot{e}_{ref}}\right)\right) \tag{20}$$

where E_{1ref}, E_{2ref} and E_{3ref} are the instantaneous moduli at a chosen reference strain-rate $\dot{\varepsilon}_{ref}$ and, s_1, s_2 and s_3 are the strain-rate sensitivity parameters.

The transition temperatures T_β, T_g and T_m are, respectively, given by:

$$\frac{1}{T_b\left(\dot{e}\right)}=\frac{1}{T_{b\,ref}}+\frac{k}{\Delta H_b}\ln\left(\frac{\dot{e}_{ref}}{\dot{e}}\right) \tag{21}$$

$$T_g\left(\dot{e}\right)=T_{gref}-c_{2g}\log\left(\frac{\dot{e}_{ref}}{\dot{e}}\right)\left(c_{1g}+\log\left(\frac{\dot{e}_{ref}}{\dot{e}}\right)\right)^{-1} \tag{22}$$

$$T_m\left(\dot{e}\right)=T_{mref}\left(1+10^{-2}\log\left(\frac{\dot{e}}{\dot{e}_{ref}}\right)\right) \tag{23}$$

in which $T_{\beta ref}$, T_{gref} and T_{mref} are the transition temperatures at the chosen reference strain-rate $\dot{\varepsilon}_{ref}$, ΔH_b is the β-activation energy and, c_{1g} and c_{2g} are the Williams-Landel-Ferry coefficients.

Fig. 3 plots the yield stress as a function of temperature.

The viscoplastic stretching rate tensor is given by the following flow rule:

$$\mathbf{D}_I^{\text{vp}} = \dot{g}_I^{\text{vp}} \frac{\boldsymbol{\sigma}_I^{\prime}}{\sqrt{2}t_I}, \quad t_I = \sqrt{\frac{1}{2}\boldsymbol{\sigma}_I^{\prime} \times \boldsymbol{\sigma}_I^{\prime}} \tag{24}$$

in which $\dot{\gamma}_I^{\text{vp}}$ is the viscoplastic shear strain rate and τ_I is the effective shear stress related to the deviatoric part of the intermolecular Cauchy stress: $\boldsymbol{\sigma}_I^{\prime} = \boldsymbol{\sigma}_I - s_{Im}\mathbf{I}$ with $s_{Im} = \text{trace}\left(\boldsymbol{\sigma}_I\right)/3$ the intermolecular mean stress and $\mathbf{I}$ the identity tensor. The expression of $\dot{\gamma}_I^{\text{vp}}$ proposed by Richeton et al. (2006, 2005a), above and below the glass transition temperature T_g, is retained:

$$\dot{g}_I^{\text{vp}} = \dot{g}_0 \exp\left(-\frac{\Delta H_b}{Rq}\right)\sinh^n\left(\frac{\left(t_I - t_i\right)V}{2kq}\right) \text{ for } q < T_g \tag{25}$$

above T_g, and

$$\dot{g}_I^{\text{vp}} = \dot{g}_0 \exp\left(-\frac{\Delta H_b}{RT_g}\right)\exp\left(\frac{\ln 10^{\prime}\, c_{1g}\left(q - T_g\right)}{c_{2g} + q - T_g}\right)\sinh^n\left(\frac{t_I V}{2kq}\right) \text{ for } q \geq T_g \tag{26}$$

below T_g. The term $\dot{\gamma}_0$ is the pre-exponential factor, R is the perfect gas constant, k is the Boltzmann's constant, V is the activation volume and n is a material constant.

The strain-softening originates from …

The term τ_i in Eq. (25) is the internal shear resistance of the stress-softening response in the glassy regime, continuously decreasing until reaching the more stable chains structure during the network rearrangement. The internal stress τ_i evolves from its initial value $t_{i(t=0)}$ to the value τ_{ps} referring to the preferred structural state of the polymer chains according to the following evolution law:

$$\dot{t}_i = h\left(1 - \frac{t_i}{t_{ps}}\right)\dot{g}_I^{\text{vp}} \tag{27}$$

in which h is the strain-softening slope.

$$t_{i(t=0)} = t_{i(q=0)} - mq + as_{Im} \tag{28}$$

where $t_{i(q=0)}$ is the internal stress at the temperature θ = 0 K, m is the sensitivity parameter vis-à-vis the temperature and a is the sensitivity parameter vis-à-vis the intermolecular mean stress σ_{Im}.

Viscohyperelastic Response: Strain Dramatic Hardening at Large Strains

The strain-hardening originates from …

The network Cauchy stress $\boldsymbol{\sigma}_N$ is expressed by the following constitutive relationship (Arruda and Boyce, 1993):

$$\boldsymbol{\sigma}_N = \frac{1}{J_N}\frac{C_r}{3}\frac{\sqrt{N_{rl}}}{\bar{l}_N^{\mathrm{h}}} L^{-1}\left(\frac{\bar{l}_N^{\mathrm{h}}}{\sqrt{N_{rl}}}\right)\bar{\mathbf{F}}_N^{\mathrm{h}}\left(\bar{\mathbf{F}}_N^{\mathrm{h}}\right)^{\mathrm{T}} - \left(\bar{l}_N^{\mathrm{h}}\right)^2\mathbf{I} \tag{29}$$

in which $J_N = \det\left(\mathbf{F}_N^{\mathrm{h}}\right)$ is the network volume change, $\bar{l}_N^{\mathrm{h}} = \sqrt{\mathrm{trace}\left(\bar{\mathbf{F}}_N^{\mathrm{h}}\left(\bar{\mathbf{F}}_N^{\mathrm{h}}\right)^{\mathrm{T}}\right)/3}$ is the average stretch on a chain, $C_r = n_c kq$ is the rubbery modulus with n_c the average number of chains per unit volume and N_{rl} is the average number of rigid links between entanglements. The inverse Langevin function is given by the approximation (Cohen, 1991): $\mathrm{L}^{-1}(x) \approx x(3 - x^2)/(1 - x^2)$.

The viscous stretching rate tensor is given by the following flow rule:

$$\mathbf{D}_N^{\mathrm{v}} = \dot{g}_N^{\mathrm{v}}\frac{\boldsymbol{\sigma}_N'}{\sqrt{2}t_N}, \quad t_N = \sqrt{\frac{1}{2}\boldsymbol{\sigma}_N' \times \boldsymbol{\sigma}_N'} \tag{30}$$

in which $\dot{\gamma}_N^{\mathrm{v}}$ is the viscous shear strain rate:

$$\dot{g}_N^{\mathrm{v}} = C\left(l_N^{\mathrm{v}} - 1\right)^{-1} t_N \tag{31}$$

where C is a material constant, λ_N^{v} is given by: $l_N^{\mathrm{v}} = \sqrt{\mathrm{trace}\left(\mathbf{F}_N^{\mathrm{v}}\left(\mathbf{F}_N^{\mathrm{v}}\right)^{\mathrm{T}}\right)/3}$ and τ_N is the effective shear stress related to the deviatoric part of the network Cauchy stress: $\boldsymbol{\sigma}_N' = \boldsymbol{\sigma}_N - s_{Nm}\mathbf{I}$ with $s_{Nm} = \mathrm{trace}\left(\boldsymbol{\sigma}_N\right)/3$.

The three constants, C_r, N_{rl} and C, follow a linear evolution with the temperature according to the following relationships:

$$\begin{aligned} C_r &= C_{r0} - aq \\ N_{rl} &= N_{rl0} + bq \\ C &= C_0 + cq \end{aligned} \quad \text{for } q \le T_g \tag{32}$$

above T_g, and

$$\begin{aligned} C_r &= \left(C_{r0} - aT_g\right)\frac{q}{T_g} \\ N_{rl} &= N_{rl0} + bT_g \\ C &= \left(C_0 + cT_g\right)\frac{q}{T_g} \end{aligned} \quad \text{for } q \ge T_g \tag{33}$$

below T_g. The terms C_{r0}, N_{rl0}, C_0, a, b and c are material constants.

In what follows, the model parameters are identified using experimental results obtained on a PMMA, deformed above and below its T_g.

Results and Discussion

Comparison between simulated model results and experimental results. In this section, we focus on identifying the parameters of the model that describe the constitutive behavior of PMMA. The following part presents a comparison between the simulation results and the experimental compression data.

Table 1. Parameter of PMMA model

Simulation results	Experimental results
E^{ref}_1 (MPa)	5100
E^{ref}_2 (MPa)	2700
E^{ref}_3 (MPa)	20
T^{ref}_β (K)	290
T^{ref}_g (K)	387
T^{ref}_f (K)	466
$\dot{e}^{\text{ref}}$ (s^{-1})	1
m_1	5
m_2	40
m_3	20
c_1	32.58
c_2	83.5
s	0.087
n	6.37
V (m^3)	$9.75 * 10^{-29}$
τ_i (0) (MPa)	100
m (MPa/K)	0.25
$\dot{\gamma}_0$ (s^{-1})	$1.16 * 10^{16}$
ΔH_β (kJ/mol)	90
$\frac{\tau_{ps}}{\tau_i}$	0.20
h (MPa/K)	30
α_p	0.26
$C_{r,0}$ (MPa)	91.15
a (MPa/K)	0.226
N_{rl}	1.515
b (1/K)	0.0025
C_m (MPa^{-1} s^{-1})	$-9 * 10^{-11}$
c (MPa^{-1} s^{-1}/K)	$1 * 10^{-11}$

Effect of Temperature

The figures below show the comparison between the simulated and experimental stress–strain curves over a wide temperature range (0°C to 100°C) and for three strain rates (10^{-1} s^{-1}, 10^{-2} s^{-1}, 10^{-3} s^{-1}). A satisfactory

correlation between the results was observed. It can be seen that the yield stress depends on both the strain rate and the temperature

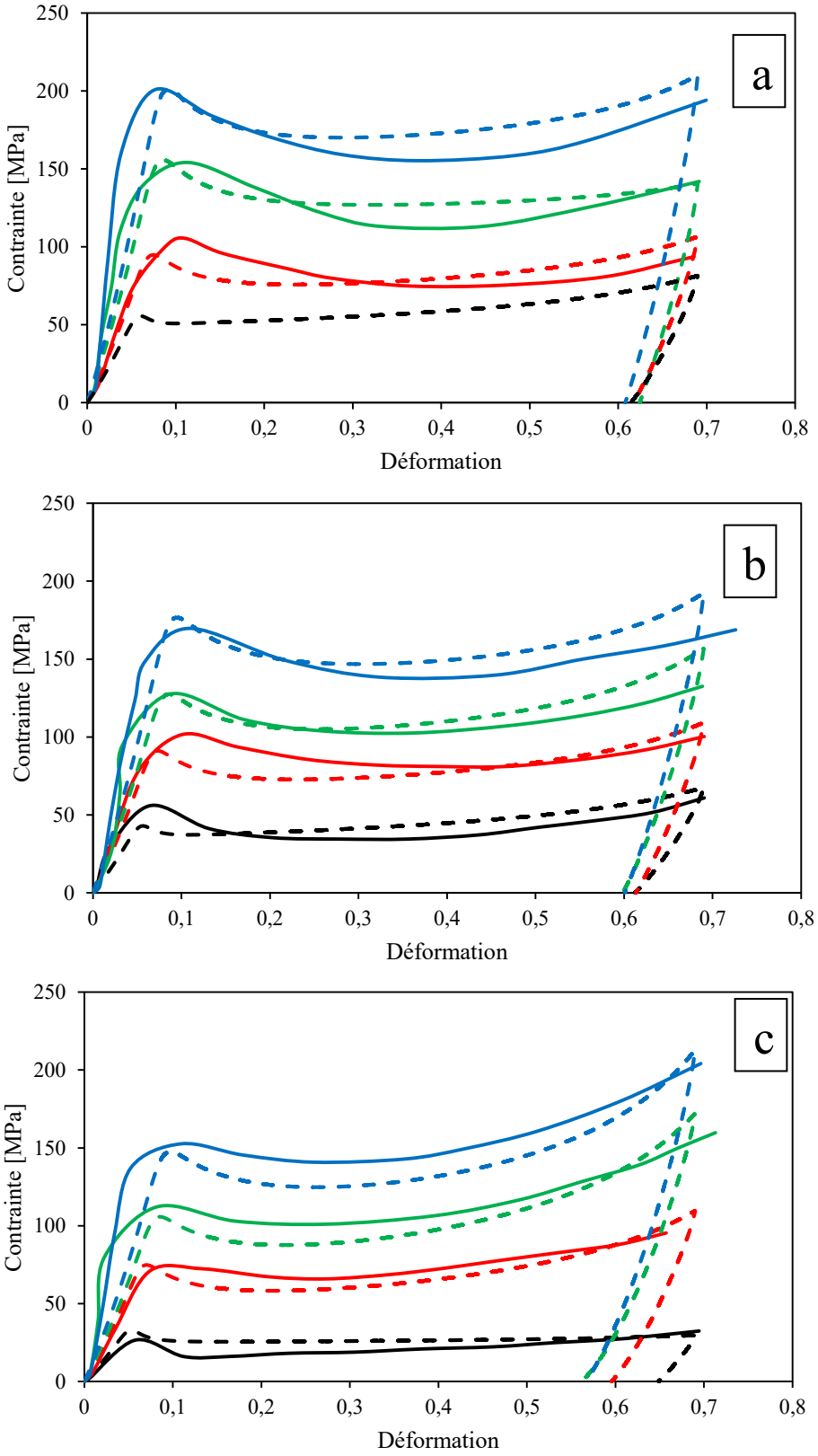

Figure 2. Model (dashed lines) vs. experiments (solid lines) of the stress-strain response of PMMA at different temperatures and strain-rates: (a) 0.01 s-1, (b) 0.001 s-1, (c) 0.0001 s

.

In fact, the model is capable of representing various curve shapes, including the initial modulus, softening after yielding, initial hardening, and excessive hardening at large deformations. It is also able to capture the effects of strain-rate and temperature sensitivity of the material during both loading and unloading.

Effect of Strain Rate

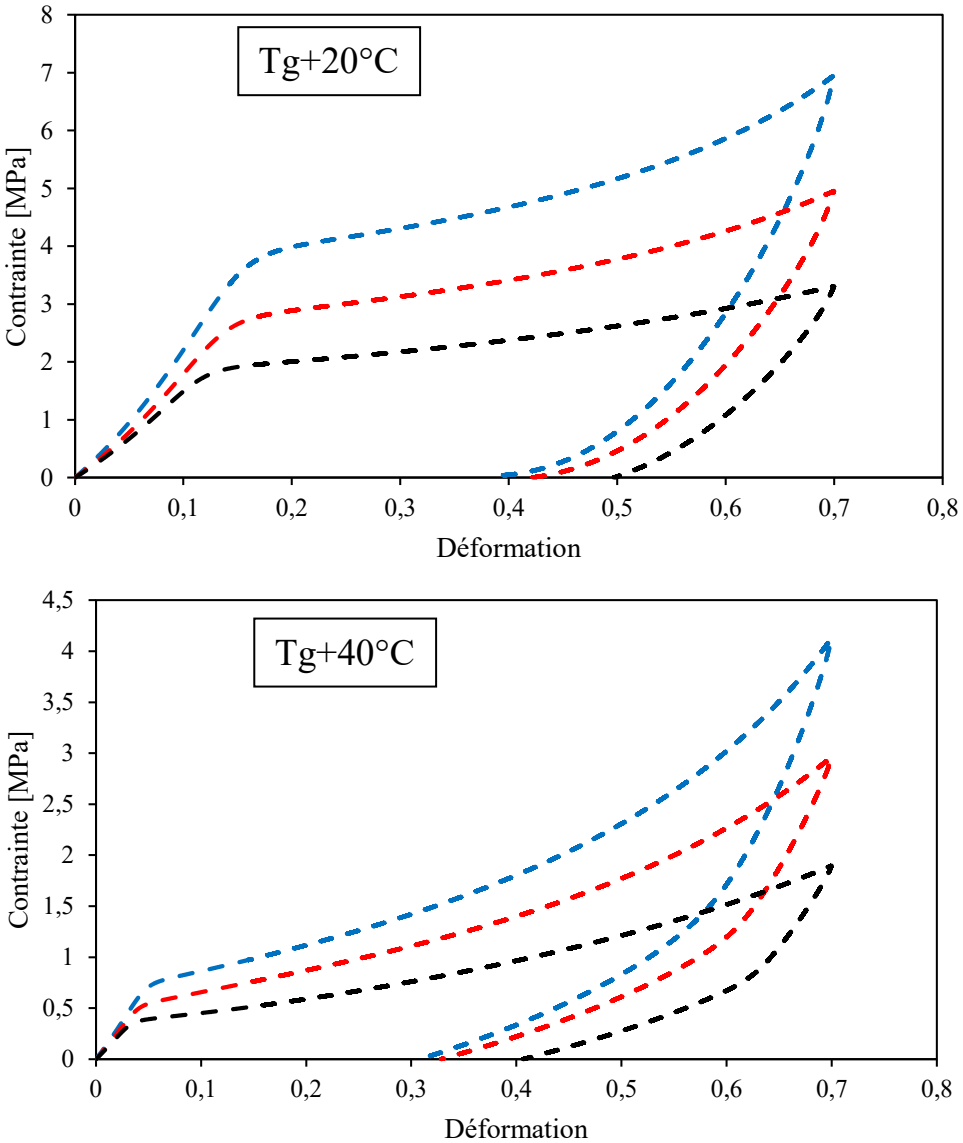

Figure 3. Model of the stress-strain response of PMMA at two different temperatures and strain-rates: (a) 0.01 s-1, (b) 0.001 s-1, (c) 0.0001 s

The two figures presented illustrate the effect of strain rate on the mechanical behavior of PMMA (Polymethyl methacrylate) at temperatures above the glass transition temperature (Tg). The higher the strain rate, the greater the stress required to achieve the same level of deformation. The curves shift upward as the strain rate increases, indicating a stiffer material response at higher loading rates. At temperatures above Tg, PMMA exhibits a pronounced viscoelastic behavior. An increase in strain rate restricts the mobility of polymer chains, thereby increasing the apparent mechanical strength.

At higher temperatures (Tg + 40°C), the stresses corresponding to a given deformation are lower than those at Tg + 20°C, indicating a decrease in stiffness with increasing temperature. Although the effect of strain rate is still present, the gap between the curves decreases at higher temperatures, reflecting a reduced sensitivity to strain rate.

Conclusion

In conclusion, we have developed a physically based model capable of capturing the elastoviscoplastic–viscohyperelastic behavior of amorphous thermoplastics, consistent with the underlying thermo-mechanical mechanisms below and above the glass transition temperature. The model accurately reproduces experimental stress–strain data for PMMA and successfully reflects the pronounced changes in mechanical response induced by temperature variations across the full range of strain rates investigated. The temperature-dependent material kinetics were then employed to simulate the thermally activated strain recovery process, and the predictive performance of the model was validated under various testing conditions. Owing to its general mathematical framework, the constitutive theory can be applied to the thermo-mechanical behavior of a wide range of amorphous thermoplastics, offering a valuable tool for predicting thermally induced strain recovery.

Scientific Ethics Declaration

* The authors declare that the scientific ethical and legal responsibility of this article published in EPSTEM journal belongs to the authors.

Conflict of Interest

* The authors declare that they have no conflicts of interest

Funding

* This research received no specific grant from any funding agency in the public, commercial, or not-for-profit sectors.

Acknowledgements or Notes

* This article was presented as a poster presentation at the International Conference on Technology, Engineering and Science (www.icontes.net) held in Antalya/Türkiye on November 12-15, 2025.

References

Arruda, E. M., & Boyce, M. C. (1993). A three-dimensional constitutive model for the large stretch behavior of rubber elastic materials. *Journal of the Mechanics and Physics of Solids, 41*(2), 389-412.

Bergström, J. S., & Boyce, M. C. (1998). Constitutive modeling of the large strain time-dependent behavior of elastomers. *Journal of the Mechanics and Physics of Solids, 46*(5), 931-954.

Boyce, M. C., Montagut, E. L., & Argon, A. S. (1992). The effects of thermomechanical coupling on the cold drawing process of glassy polymers. *Polymer Engineering & Science, 32*(15), 1073-1085.

Boyce, M. C., Parks, D. M., & Argon, A. S. (1988). Large inelastic deformation of glassy polymers. Part I: Rate dependent constitutive model. *Mechanics of Materials, 7*(1), 15-33.

Boyce, M. C., Socrate, S., & Llana, P. G. (2000). Constitutive model for the finite deformation stress–strain behavior of poly(ethylene terephthalate) above the glass transition. *Polymer, 41*(6), 2183-2201.

Boyce, M. C., Weber, G. G., & Parks, D. M. (1989). On the kinematics of finite strain plasticity. *Journal of the Mechanics and Physics of Solids, 37*(6), 647-665.

Cohen, A. (1991). A Padé approximant to the inverse Langevin function. *Rheologica Acta, 30*(3), 270-273.

Fotheringham, D., Cherry, B. W., & Bauwens-Crowet, C. (1976). Comment on "The compression yield behaviour of polymethyl methacrylate over a wide range of temperatures and strain-rates." *Journal of Materials Science, 11*(7), 1368-1371.

Holzapfel, G. A., & Simo, J. C. (1996). Entropy elasticity of isotropic rubber-like solids at finite strains. *Computer Methods in Applied Mechanics and Engineering, 132*(1–2), 17-44.

Lee, E. H. (1969). Elastic-plastic deformation at finite strains. *Journal of Applied Mechanics, 36*(1), 1-6.

Lee, E. H., & Liu, D. T. (1967). Finite-strain elastic-plastic theory with application to plane-wave analysis. *Journal of Applied Physics, 38*(1), 19-27.

Lion, A. (1997). On the large deformation behaviour of reinforced rubber at different temperatures. *Journal of the Mechanics and Physics of Solids, 45*(11), 1805-1834.

Lion, A. (2000). Constitutive modelling in finite thermoviscoplasticity: A physical approach based on nonlinear rheological models. *International Journal of Plasticity, 16*(3–4), 469-494.

Lu, S. C. H., & Pister, K. S. (1975). Decomposition of deformation and representation of the free energy function for isotropic thermoelastic solids. *International Journal of Solids and Structures, 11*(7–8), 927-934.

Mahieux, C. A., & Reifsnider, K. L. (2001). Property modeling across transition temperatures in polymers: A robust stiffness–temperature model. *Polymer, 42*(7), 3281-3291.

Mahieux, C. A., & Reifsnider, K. L. (2002). Property modeling across transition temperatures in polymers: Application to thermoplastic systems. *Journal of Materials Science, 37*(5), 911-920.

Miehe, C. (1995). Entropic thermoelasticity at finite strains. Aspects of the formulation and numerical implementation. *Computer Methods in Applied Mechanics and Engineering, 120*(3-4), 243-269.

Richeton, J., Ahzi, S., Daridon, L., & Rémond, Y. (2005). A formulation of the cooperative model for the yield stress of amorphous polymers for a wide range of strain rates and temperatures. *Polymer, 46*(16), 6035-6043.

Richeton, J., Ahzi, S., Vecchio, K. S., Jiang, F. C., & Adharapurapu, R. R. (2006). Influence of temperature and strain rate on the mechanical behavior of three amorphous polymers: Characterization and modeling of the compressive yield stress. *International Journal of Solids and Structures, 43*(7-8), 2318-2335.

Richeton, J., Ahzi, S., Vecchio, K. S., Jiang, F. C., & Makradi, A. (2007). Modeling and validation of the large deformation inelastic response of amorphous polymers over a wide range of temperatures and strain rates. *International Journal of Solids and Structures, 44*(24), 7938-7954.

Richeton, J., Schlatter, G., Vecchio, K. S., Rémond, Y., & Ahzi, S. (2005). A unified model for stiffness modulus of amorphous polymers across transition temperatures and strain rates. *Polymer, 46*(19), 8194–8201.

Sidoroff, F. (1974). Nonlinear viscoelastic model with an intermediate configuration. *Journal de Mécanique, 13*, 679–713.

Williams, M. L., Landel, R. F., & Ferry, J. D. (1955). The temperature dependence of relaxation mechanisms in amorphous polymers and other glass-forming liquids. *Journal of the American Chemical Society, 77*(14), 3701–3707.

Author(s) Information

Cherief Mohammed Nadhir Djamel Eddine
Djilali Liabes University of Sidi Bel Abbes,
Sidi Bel Abbes Algeria
Contact e-mail: *n.cherief@yahoo.com*

Ghermaoui Ilias Mohammed Amine
Djilali Liabes University of Sidi Bel Abbes,
Sidi Bel Abbes Algeria

To cite this article:

Eddine, C. M. N. D., & Amine, G. I. M., (2025). Effect of the strain rate and temperature on the shape memory behavior of PMMA. *The Eurasia Proceedings of Science, Technology, Engineering and Mathematics (EPSTEM), 38,* 264-275.